Ocean Engineering 266 (2022) 112833

Contents lists available at ScienceDirect

Ocean Engineering

journal homepage: www.elsevier.com/locate/oceaneng

Data-driven prediction and study of vortex induced vibrations by leveraging hydrodynamic coefficient databases learned from sparse sensors

Andreas P. Mentzelopoulos [a], José del Águila Ferrandis [a], Samuel Rudy [a], Themistoklis Sapsis [a], Michael S. Triantafyllou [a,*], Dixia Fan [b,*]

[a] Department of Mechanical Engineering, Massachusetts Institute of Technology, Cambridge, MA 02139, USA
[b] School of Engineering, Westlake University, Hangzhou, Zhejiang 310024, China

ARTICLE INFO

Keywords:
VIV
Vortex induced vibrations
Flexible body VIV
Flexible cylinder
Riser
Marine riser
Catenary riser
SCR
Optimization
Learning
Parametric hydrodynamic coefficient database

ABSTRACT

Semi-empirical models are currently the state-of-the-art industry tool for flexible cylinder vortex induced vibrations (VIV) fatigue prediction. Accurate prediction of the structural response relies entirely on the accuracy of the acquired hydrodynamic coefficient database. The construction of systematic hydrodynamic coefficient databases from rigid cylinder forced vibration experiments can be time-consuming for simple cases and intractable for multi-parametric cases. An alternative approach has been implemented in this work to improve the flexible cylinder VIV prediction by machine-learning optimal parametric hydrodynamic databases using physical experimental measurements. The methodology is applied to a straight riser in uniform flow and extended to non-straight riser configurations and non-uniform incoming flow profiles. Moreover, database inference is extended to using direct sparse sensor measurements along the structure. Specifically, a 19-dimensional parametric hydrodynamic coefficient database is obtained for: (i) straight riser in uniform flow (using sparse strain measurements), (ii) straight riser in sheared flow, and (iii) catenary riser in uniform flow with a 60 deg incidence angle between the catenary plane and the incoming flow stream. The predicted amplitude and frequency responses, using the extracted databases, are compared with observed experimental results.

1. Introduction

Vortex induced vibrations (VIV) have been known to engineers for hundreds of years, first observed by the ancient Greeks as "aeolian tones", sounds created by wake vortex induced pressure fluctuations as wind passes around obstacles and later sketched as vortices by Leonardo da Vinci. Extensive studies on the subject have been conducted in the last five decades; this work explores and extends the approach presented in Rudy et al. (2022). Although most studies focus on suppressing VIV due to their destructive capabilities (Park et al., 2016; Bernitsas and Raghavan, 2008; Baek and Karniadakis, 2009), attempts to harness energy from flows have also led to their study (Bernitsas et al., 2008; Lv et al., 2021; Kim et al., 2021; Bernitsas et al., 2009).

VIV affect bluff bodies in the presence of currents due to periodic vortical structures developed in the bodies' wakes (Bernitsas et al., 2019). Those vortical structures create alternating pressure variations, which synchronize with the body motion, causing persistent vibrations, which may have detrimental effects on engineered structures by causing fatigue damage (Bernitsas et al., 2019).

VIV occur across a wide range of body oscillating frequencies, known as the lock-in range, in which synchronization between vortex shedding and body motion occurs (Williamson and Govardhan, 2004; Wang et al., 2020). This synchronization occurs over a wide range of current velocities, enabled by the variability of the added mass, exhibiting a nonlinear resonance (Govardhan and Williamson, 2002). During lock-in, moderate response amplitudes occur, typically self-limited to about one diameter. The vortex shedding frequency can differ from the Strouhal frequency of a fixed cylinder because the relative motion between the vibrating cylinder and the shed vortices can significantly alter the effective fluid added mass (Wang et al., 2021a), resulting in a variable natural frequency as function of the stream velocity (Williamson, 1996).

Given the bluff shape of many offshore engineering structures, such as cables, mooring lines, and marine risers, a thorough understanding of the underlying physics of bluff body VIV is essential in controlling their effects, whether it is fatigue damage to offshore equipment or energy harnessing from flows (Bernitsas et al., 2008; Bernitsas, 2016).

* Corresponding authors.
E-mail addresses: ament@mit.edu (A.P. Mentzelopoulos), jaguila@mit.edu (J. del Águila Ferrandis), shrudy@mit.edu (S. Rudy), sapsis@mit.edu (T. Sapsis), mistetri@mit.edu (M.S. Triantafyllou), fandixia@westlake.edu.cn (D. Fan).

https://doi.org/10.1016/j.oceaneng.2022.112833
Received 30 June 2022; Received in revised form 7 September 2022; Accepted 5 October 2022
Available online 22 October 2022

Through experimental (Hover et al., 2001; Raghavan and Bernitsas, 2011; Xu et al., 2013; Fan et al., 2019a) and numerical (Evangelinos et al., 2000; Wu et al., 2014; Wang et al., 2021b; Ding et al., 2013, 2019; Raissi et al., 2019; Wu et al., 2020) methods, studies reveal that the hydrodynamic forcing on cylinders can vary significantly as the incoming flow stream velocity and the cylinder motions vary. Specifically, the forcing is greatly affected by the vortex shedding pattern.

First, VIV experiments were conducted in which a rigid cylinder was forced to oscillate in a prescribed trajectory (Sarpkaya, 1978). In particular, studies focused on the mean drag coefficient C_d, the lift coefficient in-phase with the velocity C_{lv}, and the added mass coefficient in the cross-flow (CF) direction, C_m, as functions of the true reduced velocity $V_r = \frac{U}{fD}$ and the non-dimensional CF amplitude $A^* = \frac{A}{D}$, where U is the prescribed fluid velocity; f is the prescribed motion frequency; A is the prescribed motion amplitude; and D is the cylinder's diameter. For a summary see Gopalkrishnan (1993), Sarpkaya (1995), Fan et al. (2019a). The experiments revealed that regions of positive C_{lv}, denoting net energy transferred from the fluid to the structure, were constrained to a specific range of V_r and A^*. In addition, they reported that the added mass coefficient could vary significantly assuming negative and positive values.

The measured hydrodynamic coefficients from rigid cylinder forced vibration experiments were later successfully used to predict the motions of rigid cylinder VIV, and they have served as hydrodynamic coefficient databases used to reasonably accurately predict the fluid forces in semi-empirical flexible riser VIV prediction codes (Roveri and Vandiver, 2001; Triantafyllou et al., 1999; Larsen et al., 2001).

In fluid mechanics, the added mass is described as "the entrained fluid mass" disturbed by the acceleration of a body moving through the fluid. In VIV the added mass represents the component of the forcing on the body, which is in anti-phase with acceleration; due to the presence of shed vorticity in the wake that induces forces on the body, the force is not always reactive, thus assuming positive and negative values (Fan et al., 2019b; Morse and Williamson, 2009).

The sign of the added mass strongly depends on the timing of vortex shedding; each vortex providing a suction force. Initially the excitation from the wake vortices is at the Strouhal frequency; the resulting motions, however, cause a drift to the excitation frequency, because the added mass changes, and a nonlinear "wake capture" mechanism moves the vortex formation frequency to coincide with the resulting new natural frequency (as defined by the added mass) (Sarpkaya, 1979; Triantafyllou et al., 2016). Since vortices are low pressure areas, the timing of vortex formation alters the suction force caused by the vortex on the body. If the suction force is in the direction of the body's acceleration it will reduce the inertia force resulting in a reduced added mass; if the suction force opposes the body's acceleration the apparent added mass increases.

There is also a strong correlation between the vortex shedding mode and the value of the added mass. Multiple vortex shedding modes have been reported in literature (Zdravkovich, 1996; Williamson, 1989) such as "2S", "2P", "P+S", "2P+2S", and others. For example, a "2S" shedding mode, that is two single vortices shed per period, is associated with a positive added mass while a "2P" shedding mode, which is two pairs of vortices shed, is associated with a negative added mass (Wang et al., 2021a).

The lift coefficient in phase with velocity is important because it constitutes the force that conveys energy from the fluid to the structure, or the other way around. The strong dependence of the amplitude of motion to the values of C_{lv} makes the coefficient particularly significant as it control the fatigue damage. Finally, the sign of the lift coefficient provides insight on the direction of energy transfer in the coupled flow-structure interaction problem, i.e. from fluid to structure or vice versa.

VIV of flexible bodies are similar to those of rigid bodies in the sense that the driving mechanism are also the shed vortices; the key difference is that the motion and forcing are not spanwise uniform for flexible bodies. Thus, predicting the flexible body response is significantly more challenging. Studies have been conducted to investigate the flow structure interaction of flexible bodies in VIV and revealed very complex behaviors, including various structural modes, responses of traveling waves, and recently multi-modal as well as multi-frequency vibrations (Fan, 2019; Li et al., 2022). Insights on the flow past the bodies' wakes, in which boundary layers, shear layers, vortices, and the bodies themselves interact, are currently being reported (Fan et al., 2019b; Han et al., 2018; Rudy et al., 2021a,b).

Semi-empirical models and prediction programs serve as the current state-of-the-art technology for VIV prediction (Triantafyllou et al., 1999; Larsen et al., 2001; Vandiver, 1999) although the predictive power of CFD simulations is steadily increasing and simulation accuracy is reasonably accurate in moderate size problems (Willden and Graham, 2005; Wang et al., 2018; Kamble and Chen, 2016). CFD simulations when fully resolved provide accurate results without the need for empirical information. However, at full scale Reynolds number, typically above 10^6, the computational and memory demands make fully resolved simulation challenging, while utilizing various turbulence models does not always provide reliable results for bluff body separated flows where the boundary layer transition is highly sensitive to oncoming flow turbulence, surface roughness, and Reynolds number.

Estimation of the hydrodynamic coefficients, such as the added mass coefficient C_m and the lift coefficient in phase with velocity C_{lv}, is key to the accurate prediction of the body's response using semi-empirical models. The hydrodynamic database serves as a mapping between the nondimensional amplitude, the nondimensional frequency, and the added mass and lift coefficients. Estimating the coefficients is a nontrivial process that requires performing many forced-vibration experiments with rigid cylinders, a process very expensive as well as time consuming. In addition, due to the wide input parametric space, using brute-force experiments to obtain a general hydrodynamic database, suitable for risers of various geometries in varying flow conditions, is an impossible task.

Given the high Reynolds number as well as the length scale of the field problem of risers (spanning kilometers with length to diameter ratios $L/D \approx O(10^4)$ at Reynolds numbers $Re \approx O(10^5)$) resolving full scale riser CFD simulations requires an inordinate computing effort at low Reynolds numbers and has never been done at high Reynolds numbers to the best of the authors' knowledge. There exists thus a need for developing *a new methodology to study VIV in a consistent and efficient manner*.

An alternative computational approach to studying VIV by obtaining the hydrodynamic coefficient database from data was recently proposed. This work explores and extends the new paradigm (Rudy et al., 2022) of the hydrodynamic database inference directly from the flexible body's response: an optimized parametric hydrodynamic database obtained from the comparison between experimental and semi-empirical code prediction results which could achieve a significant improvement in the predictive accuracy of semi-empirical models. The following sections illustrate how a semi-empirical forward model may be augmented by leveraging machine learning techniques to infer the hydrodynamic coefficients from data and then use the learned coefficients to make predictions or infer VIV physics.

2. Methodology

2.1. Modeling flexible body VIV

This section describes how the riser is modeled and how the modeling formulation allows for the extraction of hydrodynamic databases which may be used to then augment the forward model.

2.1.1. Eigenvalue problem

The flexible body undergoing VIV is modeled as a tensioned flexible beam with variable tension, mass properties, and geometrical properties vibrating under the excitation of a hydrodynamic force (Triantafyllou et al., 1999; Zheng et al., 2011). The equation of motion is as follows:

$$m\frac{\partial^2 y}{\partial t^2} + b\frac{\partial y}{\partial t} - \frac{\partial}{\partial x}(T\frac{\partial y}{\partial x}) + \frac{\partial^2}{\partial x^2}(EI\frac{\partial^2 y}{\partial x^2}) = f \tag{1}$$

where m is the mass per unit length, b is the damping, T is the tension on the section (and a function of the span), EI is the flexural rigidity of the body (also function of span), and f is the hydrodynamic force. The dimensions of Eq. (1) are force per unit length. We search for normal modes of vibration which are sinusoidal in time assuming the following form:

$$y(x,t) = Re\left[Y(x)e^{i\omega t}\right] \tag{2}$$

where $Y(x)$ is the complex valued amplitude of vibration along the span and ω is the cyclic frequency of vibration. The hydrodynamic force is assumed to have the following form, corresponding to a component in anti-phase with acceleration (the added mass force) and a component in phase with velocity as shown below.

$$f = Re\left[\left(\frac{1}{4}C_m\pi\rho D^2\omega^2 Y + i\frac{1}{2}C_{lv}\rho U^2 D\frac{Y}{|Y|}\right)e^{i\omega t}\right] \tag{3}$$

where Re means the "real part" (not to be confused with Reynolds number), ρ is the fluid-density, D is the body's diameter, and U is the stream velocity (assumed time invariant). The hydrodynamic coefficients C_m and C_{lv} are introduced to the model in the hydrodynamic force and their dependence on ω and Y is assumed known a priori.

By combining Eqs. (1)–(3) the following eigenvalue problem (EVP) is obtained, which may be used to determine the frequency and mode shape of the riser free vibration, i.e. under the excitation of hydrodynamic forcing only.

$$\frac{d^2}{dx^2}(EI\frac{d^2Y}{dx^2}) - \frac{d}{dx}(T\frac{dY}{dx}) + \left[-(m+\alpha C_m)\omega^2 + ib\omega\right]Y = iC_{lv}qD\frac{Y}{|Y|} \tag{4}$$

where $\alpha = \frac{1}{4}\rho\pi D^2$, and $q = \frac{1}{2}\rho U^2$. Given appropriate boundary conditions for the amplitude $Y(x)$, Eq. (4) is a well defined nonlinear eigenvalue problem. The nonlinearity originates from the dependence of the hydrodynamic coefficients C_m and C_{lv} to the amplitude $Y(x)$ and the vibration frequency ω. The EVP may be solved using an iterative nonlinear solver. The solver VIVA™ (Triantafyllou et al., 1999; Zheng et al., 2011) was used to solve the EVP.

2.1.2. The hydrodynamic coefficient database

The dependence of the hydrodynamic coefficients C_m and C_{lv} on the frequency ω and amplitude Y of the vibration is generally unknown. By accepting a "strip theory" approach, one may assume that locally (i.e. for a small section of the flexible body) the relevant nondimensional parameters for the flexible cylinder are the same as those for a rigid cylinder undergoing VIV, namely: true reduced frequency f_r, nondimensional amplitude A^*, and Reynolds number (based on diameter) Re_D.

$$f_r = \frac{\omega D}{2\pi U} \qquad A^* = \frac{A}{D} \qquad Re_D = \frac{UD}{\nu} \tag{5}$$

where ν is the fluid kinematic viscosity. The dependence of the hydrodynamic coefficients C_m and C_{lv} to the Reynolds number is rather weak (compared to the other two parameters) and may be neglected (Gopalkrishnan, 1993). Thus a complete hydrodynamic coefficient database may be defined as the mapping between:

$$C_m = f(f_r) \qquad C_{lv} = f(f_r, A^*) \tag{6}$$

Eq. (6) defines a hydrodynamic coefficient database and may be used to solve the EVP. The hydrodynamic coefficient database essentially serves as a link between the semi-empirical forcing model and reality. Given the strong evidence of the correlation between the vortex dynamics to the added mass and lift coefficients (Fan et al., 2019b; Williamson, 1996; Wang et al., 2021a), the databases may not only be used to make accurate predictions but also to understand VIV physics and to infer vortex hydrodynamics. Given that the database method is a sectional identification approach, a database is expected to remain valid for problems with similar body influences. As such is the case, a single database is used for a single riser geometry and flow condition.

Table 1
Forward model inputs and outputs.

Input	Output
Stream current profile	Amplitude response
Riser geometry and specifications	Frequency response
Hydrodynamic database	

2.2. Learning hydrodynamic coefficient databases from data

We have established a complete forward model which is able to make predictions of riser responses. We now investigate how the forward model may be combined with data (experimental, field, CFD) so that databases may be machine-learned and used to enhance the predictive accuracy of the forward model or studied to illuminate VIV physics.

2.2.1. Inverse problem definition

So far we have a forward model which given as inputs: (1) the incoming flow stream current profile, (2) the riser geometry and specifications, and (3) a hydrodynamic coefficient database, may be used to predict a riser's response. Then, provided a set of data in which: (1) the stream current profile, (2) the riser geometry, and (3) the riser response are known, the inverse prediction problem may be defined as the search for the hydrodynamic coefficient database which optimally predicts the data. Schematically this is shown in Fig. C.17 (see Table 1).

The following steps are necessary to proceed from defining the inverse problem to its mathematical formulation: (1) The hydrodynamic coefficient database must be mapped to a set of parameters which completely define it, (2) The parametric hydrodynamic coefficient database must be used with the forward model to make predictions of the (known) responses of the training data set, and (3) the parametric space defining the database must be searched in order to find the set of parameters which makes the optimal predictions according to a relevant objective.

2.2.2. Hydrodynamic feature extraction (database parametrization)

The geometry of the most extensive hydrodynamic coefficient database available, that obtained by Gopalkrishnan (1993) was used as the basis for the feature extraction (parametrization).

Given that the C_{lv} is a function of both f_r and A^*, three intermediate curves were introduced to completely define the surface's geometry. The parametrization may be visualized in Fig. 1. Contours parallel to the A^* axis, where $C_{lv} = f(A^*)$ given f_r constant (shown as blue in Fig. 1) were parametrized as two piecewise linear sections. In addition, the contour $C_{lv} = f(f_r)$ at $A^* = 0$ (shown as red in Fig. 1) and $A^*_c = f(f_r)$ (shown as purple in Fig. 1) were used and both parametrized as piecewise linear double peak curves. Corner point coordinates were used to define parameters and the shapes were smoothed using a softplus function. In a similar fashion, the added mass coefficient, C_m which is a function of f_r only was parametrized as piece-wise linear (see Fig. C.18).

Nineteen parameters ($\boldsymbol{p} : p_i,\ i \in [1,19]$) were selected in total to describe the four curves forming a complete hydrodynamic coefficient database (1. C_m vs. f_r, 2. $C_{lv,0}$ vs. f_r, 3. A^*_c vs. f_r, and 4. C_{lv} vs. A^*).

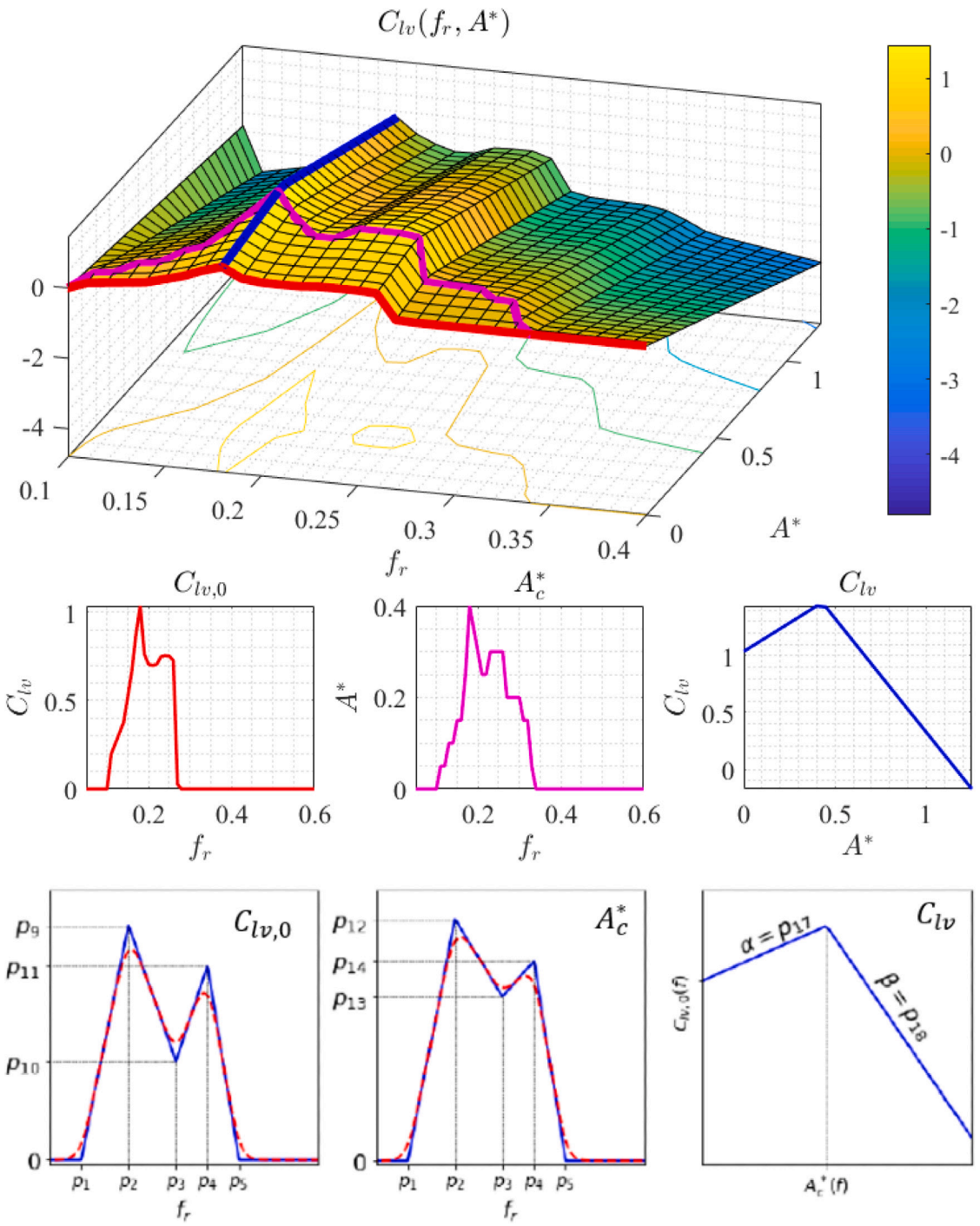

Fig. 1. (Top) Surface plot of Gopalkrishnan (1993) $C_{lv} = f(f_r, A^*)$. The projection of the surface on the $f_r - A^*$ plane is plotted. The contours used as references for the parametrization are highlighted on the surface plot. (Middle) The contours used as references for the parametrization are plotted individually. (Bottom) Shapes defined by the parametrization are illustrated. The parameters were selected to closely approximate the Gopalkrishnan (1993) C_{lv}. (For interpretation of the references to color in this figure legend, the reader is referred to the web version of this article.)

The last parameter (p_{19}) was used as the scaling factor of the softplus function.

The mathematical formulation of the parametric (reduced order) model is as follows. The softplus function is first defined:

$$sf(x, \boldsymbol{p}) = p_{19} \cdot \ln(1 + \exp\frac{x}{p_{19}}) \tag{7}$$

where p_{19} serves as a scaling constant. Then, the C_m curve may be parametrized by Eq. (8) as follows:

$$\begin{aligned}\hat{C}_m(f_r, \boldsymbol{p}) = p_{15} &+ \frac{p_{16} - p_{15}}{p_6 - p_2}[sf(f_r - p_2) - sf(f_r - p_6)] \\ &+ \frac{1 - p_{16}}{p_8 - p_7}[sf(f_r - p_7) - sf(f_r - p_8)]\end{aligned} \tag{8}$$

Table 2
Hydrodynamic feature (parameter) constraints.

p_1	$p_2 - p_8$	p_9	$p_{10} - p_{14}$	p_{15}	p_{16}	p_{17}	p_{18}	p_{19}
(0.0, 0.5)	(0,1)	(0,2)	(0,1)	(−1,1)	(1,5)	(0.1, 5)	(0.1, 5)	(0,0.005)

where $\hat{C}_m(f_r, \boldsymbol{p})$ is the parametric form of the C_m curve. The $C_{lv,0}$ may be represented parametrically as shown in Eq. (9).

$$\begin{aligned}\hat{C}_{lv,0}(f_r, \boldsymbol{p}) = &\frac{p_9}{p_2 - p_1}[sf(f_r - p_1) - sf(f_r - p_2)] \\ &+\frac{p_{10} - p_9}{p_3 - p_2}[sf(f_r - p_2) - sf(f_r - p_3)] \\ &+\frac{p_{11} - p_{10}}{p_4 - p_3}[sf(f_r - p_3) - sf(f_r - p_4)] \\ &+\frac{-p_{11}}{p_5 - p_4}[sf(f_r - p_4) - sf(f_r - p_5)]\end{aligned} \tag{9}$$

where $\hat{C}_{lv,0}(f_r, \boldsymbol{p})$ is the parametric form of the $C_{lv,0}$ curve. Accordingly, the A_c^* curve may be represented as in Eq. (10).

$$\begin{aligned}\hat{A}_c^*(f_r, \boldsymbol{p}) = &\frac{p_{12}}{p_2 - p_1}[sf(f_r - p_1) - sf(f_r - p_2)] \\ &+\frac{p_{13} - p_{12}}{p_3 - p_2}[sf(f_r - p_2) - sf(f_r - p_3)] \\ &+\frac{p_{14} - p_{13}}{p_4 - p_3}[sf(f_r - p_3) - sf(f_r - p_4)] \\ &+\frac{-p_{13}}{p_5 - p_4}[sf(f_r - p_4) - sf(f_r - p_5)]\end{aligned} \tag{10}$$

where $\hat{A}_c^*(f_r, \boldsymbol{p})$ is the parametric form of the non-dimensional critical amplitude A_c^*. Finally, the value of the lift coefficient, C_{lv} may be calculated according to Eq. (11).

$$C_{lv}(A^*, \boldsymbol{p}) = \begin{cases} C_{lv,0} + p_{17} \cdot A^* & if\, A^* \le A_c^* \\ C_{lv,0} + p_{17} \cdot A_c^* - p_{18} \cdot (A^* - A_c^*) & if\, A^* > A_c^* \end{cases} \tag{11}$$

The values of the parameters were constrained based on empirical knowledge as shown in Table 2. It should be noted that the reduced order parametric model allows for shared parameters between the 4 curves defining the complete parametric database. For instance, parameters $p_1 - p_5$ are shared between the $C_{lv,0} = f(f_r)$ and the $A_c^* = f(f_r)$ curves. The complete parametrization may be visualized in Figs. 1 and C.18.

2.2.3. Learning problem formulation

Given a complete set of parameters, a database is well defined and may be used with a forward model to make predictions of the riser's response to specific inputs. Given a set of data, the optimal set of parameters in terms of predicting the correct amplitude and frequency of motion may be searched.

We are interested in making accurate predictions of the amplitude of vibration as a function of span as well as of the frequency of vibration. Then we may formulate the objective function as follows, in order to penalize the amplitude and frequency discrepancy between observation (data) and prediction (forward model):

$$J(\boldsymbol{p}) = \sum_{i=1}^{N_{V_r}} \left[\frac{1}{L} \int_0^L |A_i - \hat{A}_i(\boldsymbol{p})| dx + \lambda |f_i - \hat{f}_i(\boldsymbol{p})| \right] \tag{12}$$

where N_{V_r} is the number of velocities tested, A is the observed amplitude, $\hat{A}(\boldsymbol{p})$ is the predicted amplitude using the parametric database, f is the vibration frequency, and $\hat{f}(\boldsymbol{p})$ is the predicted vibration frequency. The integral expression for the amplitude ensures that the discrepancy between the observed amplitude and the predicted one is minimized across the whole riser span, L. The value of the balancing factor λ was chosen arbitrarily. Fig. C.19 serves to aid the reader understand the physical meaning of the objective function.

The following regularization terms were obtained through trial and error and helped improve the results obtained using Eq. (12).

$$R(\boldsymbol{p}) = \beta \left[\frac{p_5 - p_1}{0.1} \right]^2 + \gamma |p_{19}| \tag{13}$$

where the factors β and γ are chosen arbitrarily. Specifically, the distance between parameters p_1 and p_5 compared to 0.1 was squared and penalized using a factor of β and so was the magnitude of the scaling factor of the softplus function, p_{19} using a factor of γ. Since only discrete reconstructed amplitude points across the riser's span were available, the objective function was formulated equivalently as follows:

$$\begin{aligned}J(\boldsymbol{p}) = \sum_{i=1}^{N_{V_r}} \left[\lambda \sqrt{\frac{1}{N_L} \sum_{n=1}^{N_L} [A_{i,n}^* - \hat{A}_{i,n}^*(\boldsymbol{p})]^2} + \sqrt{[f_i - \hat{f}_i(\boldsymbol{p})]^2} \right] \\ +\beta \left[\frac{p_5 - p_1}{0.1} \right]^2 + \gamma |p_{19}|\end{aligned} \tag{14}$$

where N_L is the number of points used across the span.

Obtaining riser amplitude (displacement) data is an expensive process which requires further processing of raw measured quantities (usually strain and acceleration). Since strain data are readily available from experiments or the field and in practice are much easier to obtain, it was deemed appropriate to demonstrate that the methodology can also be applied using strain data to learn hydrodynamic coefficients. In this case the objective function assumes the following form.

$$\begin{aligned}J(\boldsymbol{p}) = \sum_{i=1}^{N_{V_r}} \left[\lambda \sqrt{\frac{1}{N_L} \sum_{n=1}^{N_L} [\epsilon_{i,n} - \hat{\epsilon}_{i,n}(\boldsymbol{p})]^2} + \sqrt{[f_i - \hat{f}_i(\boldsymbol{p})]^2} \right] \\ +\beta \left[\frac{p_5 - p_1}{0.1} \right]^2 + \gamma |p_{19}|\end{aligned} \tag{15}$$

where ϵ is the observed strain directly measured on the body and $\hat{\epsilon}(\boldsymbol{p})$ is the predicted strain using the parametric database and the forward model.

2.2.4. Optimization

The objective function (Eq. (14) or Eq. (15)) is non-convex, non-smooth, and spans a 19-dimensional space. Gradient methods were ruled out since: 1. obtaining a gradient estimate requires O(10) evaluations of the forward model using finite differences (very expensive computationally) and 2. the geometry defined by the line search problem in many cases resembles a "staircase", making the gradient either very large, or almost zero.

A stochastic coordinate descent method was employed instead. Provided an estimate of the current database (i.e. a set of parameters $\boldsymbol{p}$) such that:

$$\boldsymbol{p} = (p_1,\ p_2,\ p_3, \dots,\ p_{18},\ p_{19}) \tag{16}$$

an iterative scheme was followed in which at each iteration the objective function was evaluated at several perturbations of the given estimate. Specifically, at iteration i the perturbations were of the following form:

$$\begin{aligned}\boldsymbol{p}^* &= \boldsymbol{p} + \delta_i \boldsymbol{v_i} \\ \delta_i &= \underset{\delta \in \Delta}{\arg\min}\ J(\boldsymbol{p} + \delta \boldsymbol{v_i})\end{aligned} \tag{17}$$

where $\boldsymbol{p}^*$ is the perturbed value of the parameters selected at the end of iteration i. The step size, δ_i, was drawn from $\Delta = \{0, \delta_1, \delta_2, \dots, \delta_{n_s}\}$, a set including $\{0\}$ and n_s samples of some distribution p_δ (in this case a normal distribution with geometrically decaying variance after a set number of iterations). The direction $\boldsymbol{v_i}$ was specified as either a column vector chosen from the identity matrix with randomly permuted columns or a random orthogonal matrix. In such a way the perturbation directions were not constrained to lie only along the directions of the parameters.

In order to eliminate the hard constraints posed on the optimization problem (parameter values must be in a specific range), the algorithm was performed on the transformed set of variables $\boldsymbol{q}$. The transformation from p_i to q_i was performed according to Eq. (18).

$$q_i = q_i(p_i) = \sigma^{-1}\left(\frac{p_i - p_{i,min}}{p_{i,max} - p_{i,min}}\right) \tag{18}$$

where σ is the sigmoid function and $p_{i,min}$ and $p_{i,max}$ are the minimum and maximum allowed values of each parameter p_i according to Table 2. The pseudocode for the optimization algorithm is shown in Appendix D.

2.3. Initial condition

Defining a suitable initial condition for the learning problem was deemed appropriate since initializing at random would, in the least, slow down the convergence of the optimization algorithm, and possibly be partly carried down to the converged result in regions with not many training data. The physics-informed database obtained by Gopalkrishnan (1993) which has been obtained via rigid cylinder forced vibrations was selected as the appropriate initial condition.

In order to determine the set of initial parameters $\boldsymbol{p_0}$ which optimally parametrize the Gopalkrishnan (1993) database, an optimization problem was formulated to minimize the discrepancy between the $C_{lv} = f(f_r, A^*)$ of the Gopalkrishnan (1993) database and the initial parametric database defined by $\hat{C}_{lv} = f(f_r, A^*, \boldsymbol{p_0}), \hat{C}_m = f(f_r, \boldsymbol{p_0})$. The objective function to be minimized in this context is as follows:

$$J(\boldsymbol{p}) = \int_{A^*_{min}}^{A^*_{max}} \int_{f_{r_{min}}}^{f_{r_{max}}} |C_{lv}(f_r, A^*) - \hat{C}_{lv}(f_r, A^*, \boldsymbol{p})| \; df_r \; dA^* \tag{19}$$

The integral expressions in Eq. (19) may be discretized and scaled leading to the discrete equivalent optimization expression given in Eq. (20).

$$J(\boldsymbol{p}) = \sum_{i=1}^{N_{A^*}} \sum_{j=1}^{N_{f_r}} \frac{\sqrt{\left[C_{lv}(f_{r_j}, A^*_i) - \hat{C}_{lv}(f_{r_j}, A^*_i, \boldsymbol{p})\right]^2}}{N_{f_r} \cdot N_{A^*}} \tag{20}$$

where N_{f_r} and N_{A^*} are the number of reduced frequencies and number of non-dimensional amplitudes used, respectively. The evaluation of the lift coefficient of the Gopalkrishnan database was interpolated at the centers of the grid points and a regularization term penalizing the magnitude of the scaling factor of the softplus function (p_{19}) was added. The final objective expression was:

$$J(\boldsymbol{p}) = \sum_{i=1}^{N_{A^*}-1} \sum_{j=1}^{N_{f_r}-1} \frac{\sqrt{\left[C_{lv}\left(\frac{f_{r_j}+f_{r_{j+1}}}{2}, \frac{A^*_i+A^*_{i+1}}{2}\right) - \hat{C}_{lv}\left(\frac{f_{r_j}+f_{r_{j+1}}}{2}, \frac{A^*_i+A^*_{i+1}}{2}, \boldsymbol{p}\right)\right]^2}}{N_{f_r} \cdot N_{A^*}} + \beta\sqrt{(p_{19})^2} \tag{21}$$

where the value of the balancing factor β was chosen arbitrarily.

3. Results and discussion

The goal of the learning problem was to determine the parametric hydrodynamic coefficient database which optimally predicts the riser's vortex induced cross-flow vibration responses given a set of known data. To aid the process, an appropriate initial condition for the optimization algorithm was determined. In order to assess the success of the learning problem on the various training data sets, the riser's temporal root mean square (rms) amplitude at each location across the span, as well as the vibration frequency predicted using the optimal parametric databases were compared with the observed responses.

3.1. Initial condition

The resulting C_{lv} contour as well as the training contour (that of Gopalkrishnan (1993)) are shown in Fig. 2. The optimization was performed across the range of $f_r = [0.1, 0.3]$ and $A^* = [0, 1.2]$, where most observed VIV responses occur. The initial condition C_{lv} contour qualitatively agrees with the training database both in terms of magnitude and contour shape in that region.

For low f_r, close to 0.1 the behavior the Gopalkrishnan contours is not well approximated, as the model is unable to capture the sharp corners of the training set. In addition there is a small region defined by $f_r \approx 0.15$ and $A^* \approx [0.4 - 0.6]$ where the parametric initial condition overestimates the Gopalkrishnan database C_{lv} by about 0.5. Discrepancy is also observed for $f_r > 0.3$, especially for the negative valued contours (outside the optimization range). Given that VIV occurs at a range of approximately $f_r \in [0.15, 0.30]$ where the parametrization matches the training data closely, the initial condition was deemed adequate, especially since further refinement would follow during training.

3.1.1. Uniform riser in uniform flow

The first application of the methodology included reproducing the results by Rudy et al. (2022) for a uniform cylinder in uniform flow with the obtained initial condition and extending the framework to using direct strain measurements.

Training was done on data obtained from bare cylindrical riser experiments conducted as part of the Norwegian Deep Water Programme (NDP) (Braaten and Lie, 2005). The riser specifications are shown in Table B.3. The test numbering and the corresponding flow velocities are shown in Table B.4. The tested Reynolds numbers were in the range $Re_D \approx 7.1 \cdot 10^3 - 5.7 \cdot 10^4$. The prediction results using displacement data for training are included in Appendix A.1.

Strain measurements are raw data readily available from experiments or field data. However, the number of strain gauges is limited and usually (especially in the field) strain sensing is notoriously sparse. By sparse, in this context it is meant that direct strain measurements were made at N = 24 uniformly spaced points along the span, compared to the N = 900 (reconstructed) displacement points available along the span; the difference is of one order of magnitude. Additionally, no computational complexity is added when using (raw) strain data compared to displacement data which need to be reconstructed.

Although training was done using direct strain measurements (and according to Eq. (15)), the quality of the extracted database was measured by comparing the predicted displacement of the riser as well as the frequency response. The results obtained by comparing the observed and predicted amplitude response of the riser using the strain trained database are shown in Fig. 3.

Fig. 3 includes plots of the riser's temporal rms amplitude (nondimensionalized by the diameter) as a function of span (nondimensionalized by the riser's length). The amplitude is plotted on the y-axis while the spanwise position is plotted on the x-axis. The observed (experimental) responses are plotted as solid blue curves while the predictions are plotted as a solid black curves. Each different subplot corresponds to a different flow velocity as outlined in Table B.4 (flow velocity increases from top left to bottom right).

As Fig. 3 illustrates, there is good agreement between the observed and predicted amplitude; the high mode number is also predicted. The average absolute error across the span is less than 20% of the riser's diameter (see Fig. A.14); however, in some cases, the predictions underestimate the variation of the amplitude around midspan. For low flow velocities, the observed response from the experiments is very asymmetric; in theory we expect a completely symmetric response since this is a symmetric problem. Imperfections in the setup/procedure excite an asymmetrical response which is beyond the predicting capabilities of our model. For higher flow velocities however the predictions

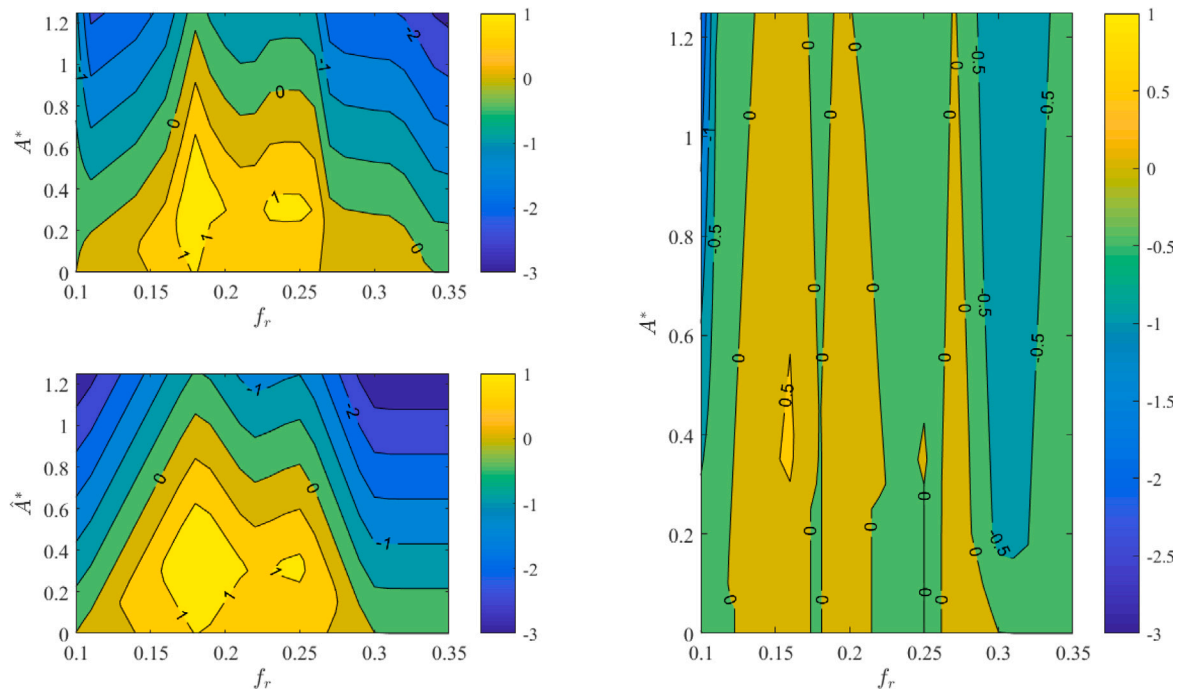

Fig. 2. Initial condition: C_{lv} contour of Gopalkrishnan database (top left) and $\hat{C}_{lv}$ contour of initialized parametric database (bottom left). The difference $\hat{C}_{lv} - C_{lv}$ is plotted on the right. The selected initial condition approximates the training contour well both in terms of magnitude and shape in the training region $f_r \in [0.1, 0.3]$.

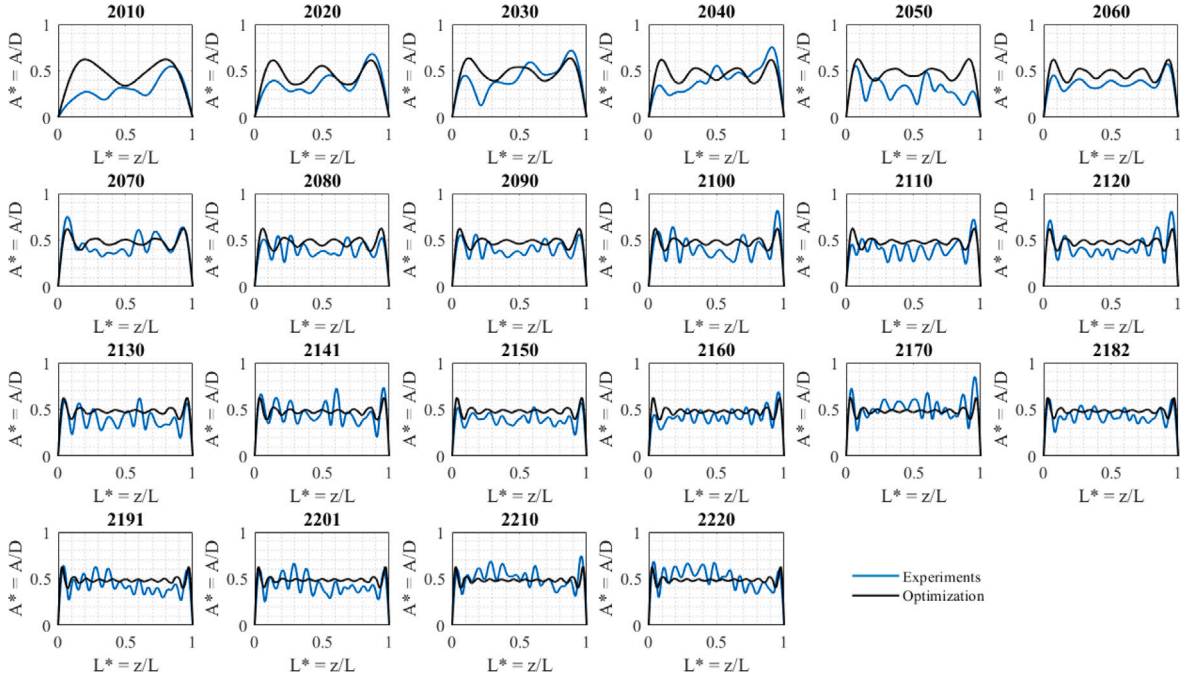

Fig. 3. Amplitude predictions for uniform riser in uniform flow (*using strain* for training). The amplitude (nondimensionalized by the cylinder's diameter) is plotted on the y-axis. The spanwise position is plotted on the x-axis. Predictions are plotted as solid black curves, while observed responses from experiments are plotted as blue curves. The predictions agree with observations well and the high mode number is predicted indicating that the strain trained database has strong predicting capabilities. (For interpretation of the references to color in this figure legend, the reader is referred to the web version of this article.)

remain accurate although perhaps slightly overestimating the response on average.

The riser frequency responses are plotted in Fig. 4. The response frequency is plotted on the y-axis while the stream velocity is plotted on the x-axis. The observed response (experimental) is plotted as a blue circle while the prediction using the extracted database is plotted as an black plus sign.

As is evident in Fig. 4, the frequency of vibration is well predicted as a function of the incoming stream velocity and the linear increasing trend is captured. For high flow velocities (i.e. about 2 m/s or higher) the predictions become gradually worse than those for low flow velocities with a maximum relative error of about 15%.

The prediction results using the extracted database using direct sparse strain measurements demonstrates how databases need not be learned from displacement data which are rather expensive to obtain

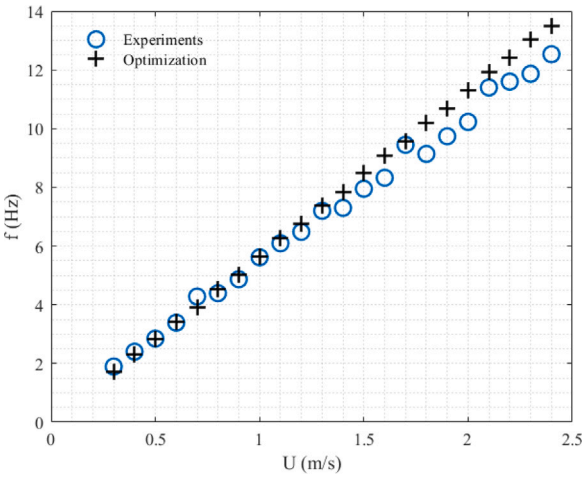

Fig. 4. Uniform cylinder in uniform flow frequency prediction (*using strain* for training). Frequency is plotted on the *y*-axis while flow velocity is plotted on the *x*-axis. Predicted responses are plotted as black plus signs while observed responses from experiments are plotted as blue circles. Good agreement is evident between observation and prediction.

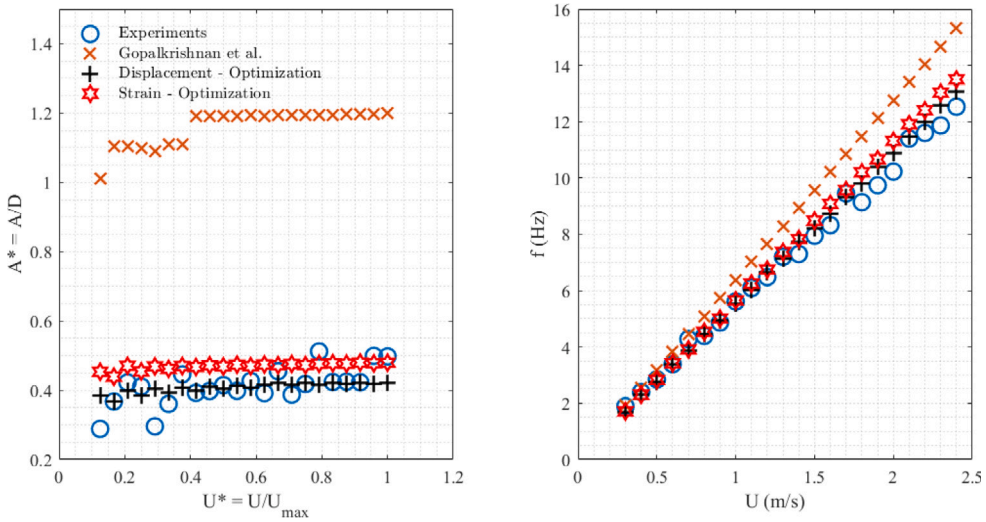

Fig. 5. Average (across the span) rms amplitude prediction as a function of nondimensional flow velocity (left) and frequency prediction as a function of velocity (right). On the left, predictions using three different databases in conjunction with the forward model are shown in addition to the experimental observations (blue circles). Specifically, predictions are made using the database obtained by Gopalkrishnan (1993) (orange x), the database extracted using displacement data for training (black +), and the database extracted using strain data for training (red hexagons). Both the displacement and the strain trained databases, which were learned from the data, have greater predicting capabilities compared to the Gopalkrishnan (1993) database which was obtained via the traditional forced vibration experiment method.

but may be determined directly from sparse strain measurements along the structure which are in practice easier to obtain.

3.1.2. Displacement vs. strain training

The learning problem was formulated using data from the NDP experiments for a straight uniform riser in uniform flow. Two different optimizations were performed on the same set of experimental data, one displacement based, and the second strain based; in both cases, reconstructed amplitude was compared to predicted amplitude and so was frequency. It should be noted that $N_L = 900$ data points across the riser's span were used for training with displacement data whereas $N_L = 24$ data points across the riser's span were used for training using strain data. In both cases, there is agreement between experimental observation and forward model prediction with the results remaining consistent regardless of training method.

A useful measure of comparison would be plotting the time–space averaged amplitude across the riser's span against the stream velocity as predicted by the two extracted databases as well as the predicted frequency as a function of the stream velocity. This is shown in Fig. 5; the figure also includes the predictions of the forward model using the Gopalkrishnan (1993) database which was also used as the initial condition for the learning problem.

Fig. 5 reveals that both the amplitude and the frequency are better predicted after optimizing the hydrodynamic coefficient database and results are consistent regardless of optimization method. In addition, the figure illustrates how the predictions deviate significantly from those made using the initial condition (i.e. Gopalkrishnan, 1993), which means that the databases were refined during training. It seems like the displacement trained database makes predictions slightly superior to those of the strain trained database although the difference is small and remains less than 10% of the diameter in most cases.

Fig. 6 shows the amplitude prediction using the extracted hydrodynamic coefficient databases for experiment 2060, as well as the prediction using the Gopalkrishnan database (Gopalkrishnan, 1993) and the observed response from experiments. As is evident in Fig. 6, the optimized hydrodynamic database, regardless of optimization method (be that displacement or strain) significantly improves the predictive power of the forward model compared to that of using the Gopalkrishnan database. Not only is the amplitude magnitude prediction more accurate but also the mode number and shape is corrected (to some

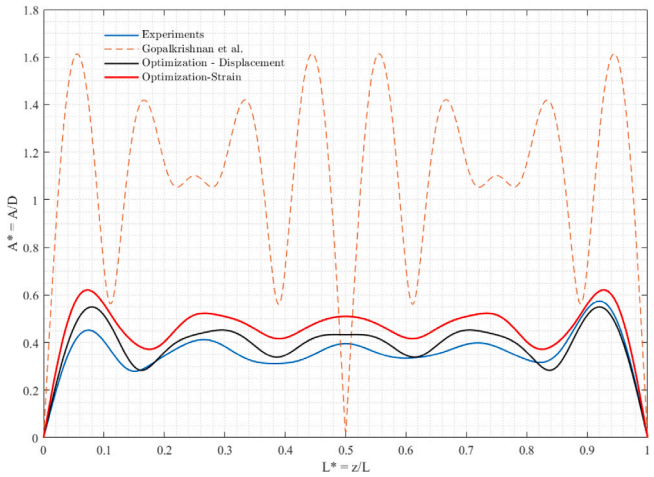

Fig. 6. Nondimensional amplitude prediction (y-axis) as a function of spanwise position (x-axis) for experiment 2060. Both in terms of amplitude and mode shape the databases obtained by the proposed framework outperform that of Gopalkrishnan (1993) obtained via the traditional forced vibration experiment method.

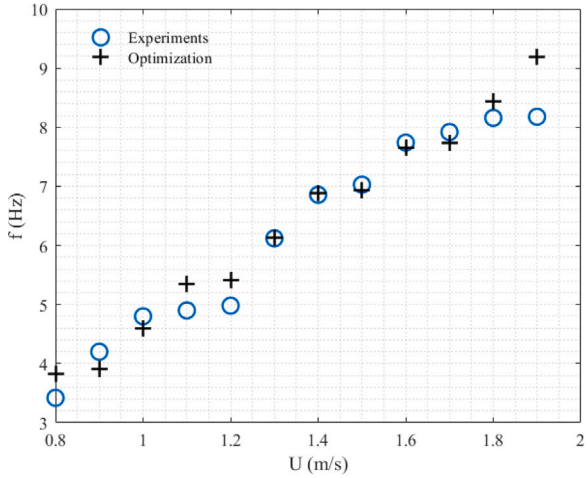

Fig. 7. Uniform cylinder in sheared flow frequency prediction. Frequency is plotted on the y-axis while flow velocity is plotted on the x-axis. Predicted responses are plotted as black plus signs while observed responses from experiments are plotted as blue circles. Agreement between observation and prediction is evident.

extent), revealing that information regarding the physics which the model was agnostic to prior to the optimization was learned during training.

The results serve to show how the extracted hydrodynamic databases make better predictions than those using the Gopalkrishnan (1993) database which was obtained via the traditional rigid cylinder forced vibration experiment method. Albeit slightly less accurate, in terms of computational complexity, the strain based method is advantageous in the sense that it does not require reconstructing the displacement which is computationally expensive.

3.2. Uniform flexible riser in sheared flow

Provided that ocean currents are non-uniform and usually better approximated by a shear or exponential profile, the methodology was applied to linear triangular shear data provided by the NDP experiments (Braaten and Lie, 2005). The riser particulars are specified in Table B.3. The test numbers and associated flow velocities are specified in Table B.5. The Reynolds number (maximum along the span) were in the range $Re_D \approx 1.9 \cdot 10^4 - 4.5 \cdot 10^4$.

Linear shear introduces non-uniformity of the flow as seen by the structure and accordingly the expected amplitude of vibration across the span is no longer expected to be symmetric. The hydrodynamic coefficient database for the shear flow case was extracted using displacement data.

As far as the frequency response is concerned, good agreement is evident between observed and predicted frequencies for the shear flow cases as is shown in Fig. 7 with relative errors of less than 15% at most.

The results for the amplitude response of the flexible cylinders are shown in Fig. 8. As Fig. 8 reveals, the learned database was able to predict the response to good accuracy across the whole span, and in addition capture the expected non-symmetrical response of the flexible structure across the full range of velocities tested. Although on a spanwise average basis responses are predicted with errors of less than 10% of the riser's diameter, the variation of the amplitude response prediction could be improved as the "wavy" shape of the observed responses is predicted as more linear.

Another result obtained from the analysis of the shear flow data is the predicted C_{lv} for the riser as a function of its span. Fig. 9 illustrates the C_{lv} as a function of span for experiment 2440; the C_{lv} is plotted as a blue solid line with the C_{lv} value plotted on the x-axis while the y-axis shows the location along the riser.

The C_{lv} as a function of the span seems to "switch" sign, from positive to negative, at approximately mid-span of the riser. This provides insight in the physics of the problem suggesting that about half the riser is absorbing energy from the flow initiating the vibrations while the other half is dissipating energy back into the fluid. This is a well understood result that may be explained as follows: the structure's half which sees the high amplitude flow velocity gets excited and initiates the vibrations, a traveling wave response is induced with waves traveling from the high velocity region to the low velocity region. At the low velocity region, the traveling wave response is dampened, transferring some energy back to the fluid. This result is of notable importance to show that the proposed methodology may not only be used to make VIV response predictions but may also serve as a tool to study the underlying physics of VIV.

3.3. Catenary flexible riser in uniform flow

Predicting the response of non straight risers is significantly more challenging since the hydrodynamics of the problem change as a function of the structure's span and the structural non-uniformity, i.e. geometric curvature, needs to be considered. As in the straight riser configurations, the tension along the structure varies and in the case of a catenary riser so does the incidence angle of the incoming flow along the span. Finally, allowing the catenary plane to be at an angle with respect to the incoming flow introduces a three-dimensional curvature

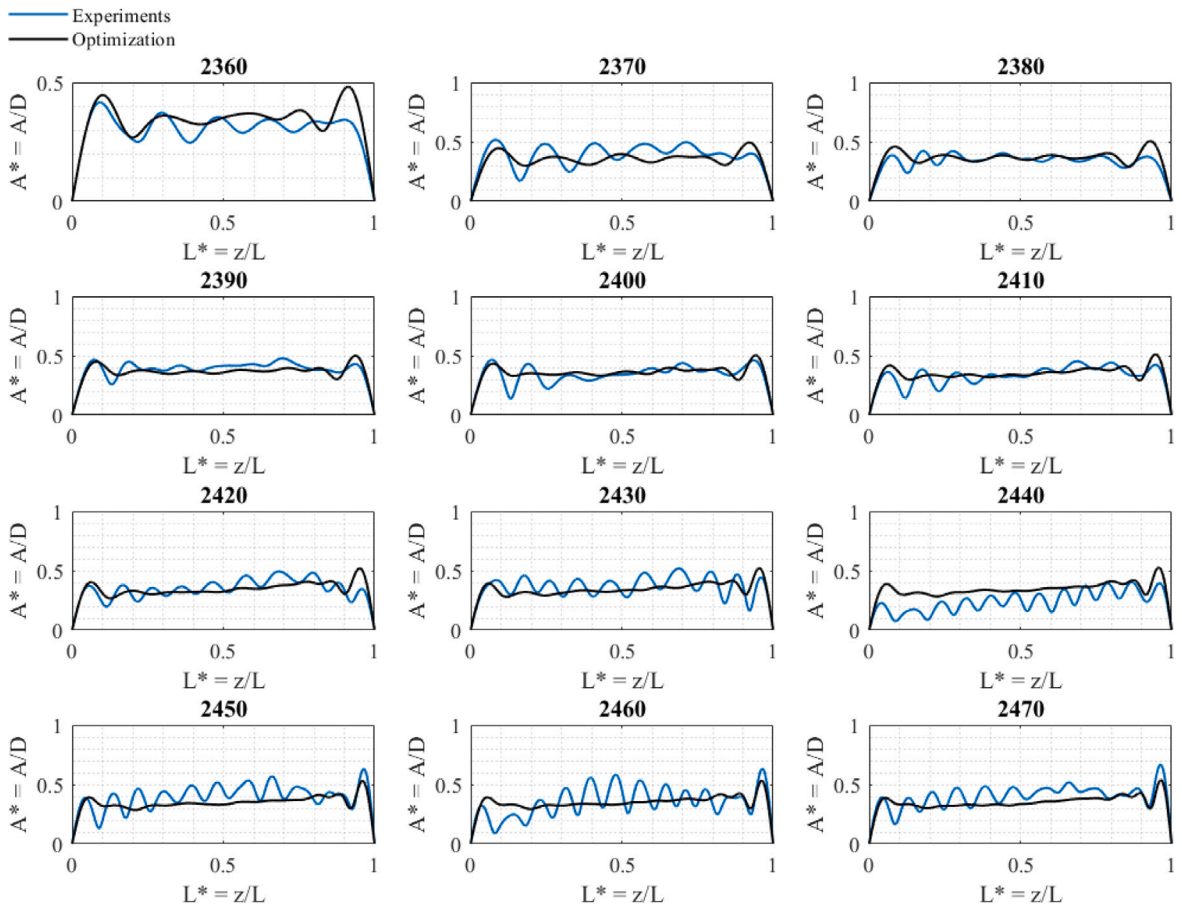

Fig. 8. Amplitude predictions for uniform riser in sheared flow. The amplitude (nondimensionalized by the cylinder's diameter) is plotted on the y-axis. The spanwise position is plotted on the x axis. Predictions are plotted as solid black curves, while observed responses from experiments are plotted as blue curves. Good agreement is observed on the general trend although the variation of the amplitude around midspan is underestimated. (For interpretation of the references to color in this figure legend, the reader is referred to the web version of this article.)

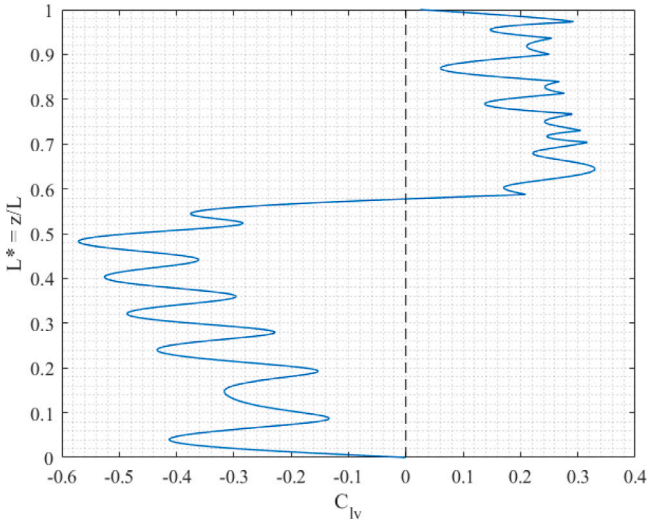

Fig. 9. Lift coefficient as a function of span for experiment 2440. Lift coefficient is plotted on the x-axis while spanwise position is plotted on the y-axis. A positive region of the C_{lv} is observed at the high velocity end of the riser; vibrations are initiated in this region and energy is absorbed from the flow. The region of negative C_{lv} corresponds to the low velocity end of the riser which is dampened transferring some energy back into the fluid.

as the steady current force is combined vectorially with the weight of the riser which increase the complexity. Fig. C.20 serves to aid the reader in understanding the experimental setup for the catenary riser.

Data from the NDP (Braaten and Lie, 2005) experiments were used. The catenary riser's particulars are detailed in Table B.6. Test numbers and corresponding flow velocities are shown in Table B.7. The Reynolds numbers were in the range $Re_D \approx 1.5 \cdot 10^3 - 4.2 \cdot 10^3$. In this and the following sections the terms "catenary riser" and "SCR riser" (usual industry abbreviation for steel catenary riser) will be used interchangeably and will refer to the catenary riser used in the NDP experiments.

The incidence angle between the catenary plane and the incoming flow stream was 60 deg. Note that the CF direction remains unchanged and is defined as the direction perpendicular to the flow velocity, rather than the direction perpendicular to the catenary plane.

The amplitude response of the SCR riser is shown in Fig. 10. On average the response amplitude is predicted with errors of less than 5% of the cylinder's diameter (see Fig. A.16) with the mode number consistently predicted to within 1. The mode shape as well as the amplitude variation across the span are also well predicted.

Fig. 11 shows the frequency responses; as is evident in the figure, the frequency is well predicted by the trained forward model. In all cases, the response is predicted to with 15% of its true value and in most cases the relative error does not exceed 10%. Moreover, the frequency "jumps" observed, which correspond to increases in the mode number were also accurately predicted.

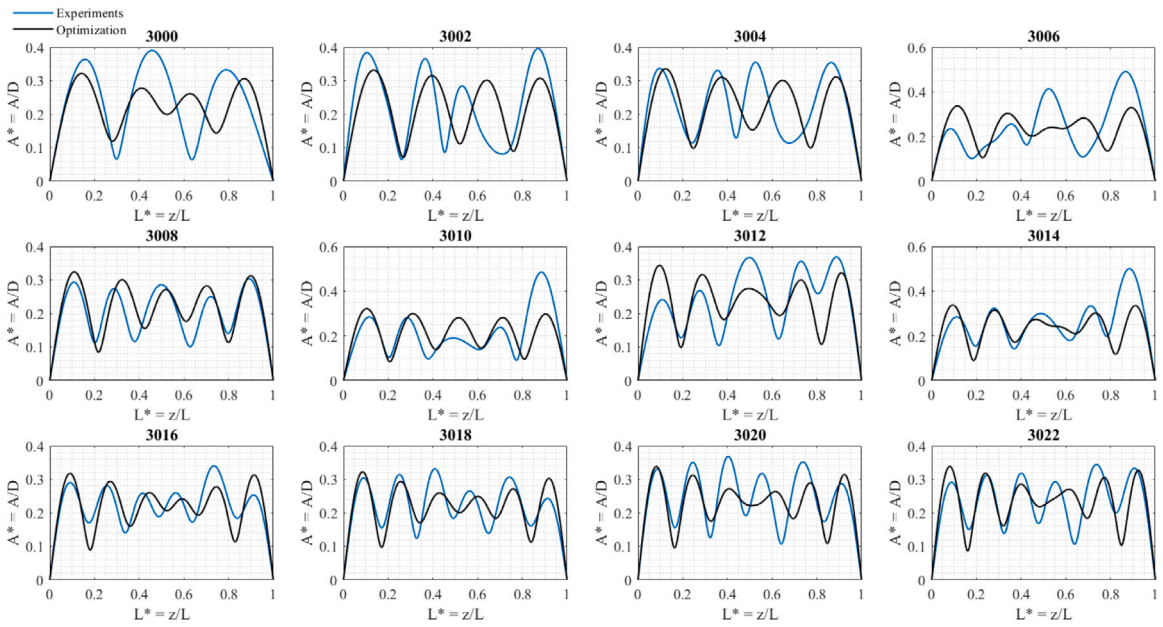

Fig. 10. Amplitude prediction for SCR riser at 60 deg incidence angle between the catenary plane and the incoming flow. The amplitude (nondimensionalized by the cylinder's diameter) is plotted on the *y*-axis. The spanwise position is plotted on the *x* axis. Predictions are plotted as solid black curves, while observed responses from experiments are plotted as blue curves. Good agreement is evident both in terms of magnitude and mode shape. (For interpretation of the references to color in this figure legend, the reader is referred to the web version of this article.)

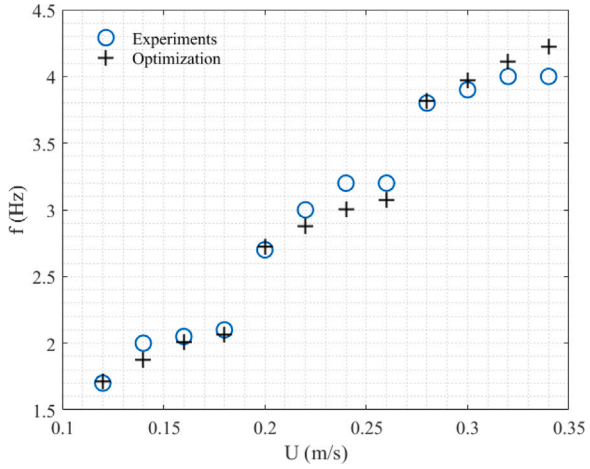

Fig. 11. Frequency prediction for SCR riser at 60 deg incidence angle between the catenary plane and the incoming flow. Frequency is plotted on the *y*-axis while flow velocity is plotted on the *x*-axis. Predicted responses are plotted as black plus signs while observed responses from experiments are plotted as blue circles. The frequency and mode jumps are well predicted.

4. Conclusion

Accurate prediction of the structural response of flexible bodies in VIV relies heavily on the quality of the obtained hydrodynamic coefficient database used to solve the coupled flow/structure interaction problem. Traditionally, databases were obtained via rigid-cylinder forced vibration experiments, a method very expensive and time consuming. Computational fluid dynamics simulations are not yet capable of resolving full scale risers and thus there exists a need for developing a methodology to infer databases which may be used not only to make accurate predictions but also to illuminate underlying VIV physics.

The methodology presented in this work extends (Rudy et al., 2022) and provides an alternative way of studying vortex induced vibrations of flexible structures, by machine-learning the hydrodynamic coefficients used to solve the coupled flow/structure interaction problem from experimental data. The proposed framework is applied to a uniform riser in both a uniform and a sheared flow and then to a catenary riser in uniform flow. An appropriate initialization for the optimization problem is also determined. Last but not least, the framework is extended to using direct sparse sensor measurements along the structure.

The uniform flow results not only validate Rudy et al. (2022) but also verify that the extracted databases are capable of making predictions superior to those made using databases obtained via the traditional rigid cylinder forced vibration experiment method. In addition, the strain trained results with appropriate initialization serve to show that the hydrodynamic coefficients may be learned while eliminating the complexity of reconstructing the riser's displacement. Moreover, the sheared flow lift coefficient result demonstrates how the framework may be used to explain VIV physics. Last but not least, the methodology is successfully applied to a catenary riser with a 60 deg angle between the catenary plane and the incoming flow stream.

A final remark is that given data sets of riser motions in the order of O(10 GB), extracting a database requires less than 24 h (on a plain computer), while individual predictions (given an extracted database) require less than 5 s (on a plain computer). Thus, the proposed framework requires orders of magnitudes less time and computing resources than higher fidelity models of greater complexity, yet still providing reasonably accurate results.

CRediT authorship contribution statement

Andreas P. Mentzelopoulos: Conceptualization, Software, Validation, Formal analysis, Writing – Original Draft, Writing – review & editing, Visualization. **José del Águila Ferrandis:** Conceptualization, Software, Data curation, Writing – review & editing. **Samuel Rudy:** Conceptualization, Methodology, Software, Formal analysis, Writing – review & editing, Visualization. **Themistoklis Sapsis:** Conceptualization, Methodology, Resources, Supervision, Writing – review & editing. **Michael S. Triantafyllou:** Conceptualization, Methodology, Software, Resources, Writing – review & editing, Supervision, Project Administration, Funding acquisition. **Dixia Fan:** Conceptualization, Methodology, Software, Formal analysis, Writing – Original Draft, Writing – review & editing, Visualization, Supervision.

Declaration of competing interest

The authors declare that they have no known competing financial interests or personal relationships that could have appeared to influence the work reported in this paper.

Data availability

Data will be made available on request.

Acknowledgment

The authors would like to acknowledge the support of the DigiMaR consortium.

Appendix A. Supplementary results

Supplementary material related to this article can be found online at https://doi.org/10.1016/j.oceaneng.2022.112833.

References

Baek, H., Karniadakis, G.E., 2009. Suppressing vortex-induced vibrations via passive means. J. Fluids Struct. 25 (5), 848–866.

Bernitsas, M.M., 2016. Harvesting energy by flow included motions. In: Springer Handbook of Ocean Engineering. Springer, pp. 1163–1244.

Bernitsas, M.M., Ben-Simon, Y., Raghavan, K., Garcia, E., 2009. The VIVACE converter: Model tests at high damping and Reynolds number around 105. J. Offshore Mech. Arct. Eng. 131 (1).

Bernitsas, M.M., Ofuegbe, J., Chen, J.-U., Sun, H., 2019. Eigen-solution for flow induced oscillations (VIV and galloping) revealed at the fluid-structure interface. In: ASME 2019 38th International Conference on Ocean, Offshore and Arctic Engineering. American Society of Mechanical Engineers Digital Collection.

Bernitsas, M.M., Raghavan, K., 2008. Reduction/suppression of VIV of circular cylinders through roughness distribution at 8× 103< Re< 1.5× 105. In: International Conference on Offshore Mechanics and Arctic Engineering, Vol. 48227. pp. 1001–1005.

Bernitsas, M.M., Raghavan, K., Ben-Simon, Y., Garcia, E., 2008. VIVACE (Vortex Induced Vibration Aquatic Clean Energy): A new concept in generation of clean and renewable energy from fluid flow. J. Offshore Mech. Arct. Eng. 130 (4).

Braaten, H., Lie, H., 2005. NDP Riser High Mode VIV Tests Main Report. MARINTEK Report, Trondheim, Norway.

Ding, L., Bernitsas, M.M., Kim, E.S., 2013. 2-D URANS vs. experiments of flow induced motions of two circular cylinders in tandem with passive turbulence control for 30,000< Re< 105,000. Ocean Eng. 72, 429–440.

Ding, W., Sun, H., Xu, W., Bernitsas, M.M., 2019. Numerical investigation on interactive FIO of two-tandem cylinders for hydrokinetic energy harnessing. Ocean Eng. 187, 106215.

Evangelinos, C., Lucor, D., Karniadakis, G., 2000. DNS-Derived force distribution on flexible cylinders subject to vortex-induced vibration. J. Fluids Struct. 14 (3), 429–440.

Fan, D., 2019. Mapping the Hydrodynamic Properties of Flexible and Rigid Bodies Undergoing Vortex-Induced Vibrations (Ph.D. thesis). Massachusetts Institute of Technology.

Fan, D., Jodin, G., Consi, T.R., Bonfiglio, L., Ma, Y., Keyes, L.R., Karniadakis, G.E., Triantafyllou, M.S., 2019a. A robotic intelligent towing tank for learning complex fluid-structure dynamics. Sci. Robot. 4 (36).

Fan, D., Wang, Z., Triantafyllou, M.S., Karniadakis, G.E., 2019b. Mapping the properties of the vortex-induced vibrations of flexible cylinders in uniform oncoming flow. J. Fluid Mech. 881, 815–858.

Gopalkrishnan, R., 1993. Vortex-Induced Forces on Oscillating Bluff Cylinders (Ph.D. thesis). Massachusetts Institute of Technology.

Govardhan, R., Williamson, C., 2002. Resonance forever: Existence of a critical mass and an infinite regime of resonance in vortex-induced vibration. J. Fluid Mech. 473, 147–166.

Han, Q., Ma, Y., Xu, W., Fan, D., Wang, E., 2018. Hydrodynamic characteristics of an inclined slender flexible cylinder subjected to vortex-induced vibration. Int. J. Mech. Sci. 148, 352–365.

Hover, F., Tvedt, H., Triantafyllou, M., 2001. Vortex-Induced Vibrations of a Cylinder with Tripping Wires. Cambridge University Press.

Kamble, C., Chen, H.-C., 2016. CFD prediction of vortex induced vibrations and fatigue assessment for deepwater marine risers. Ocean Syst. Eng. 6 (4), 325–344.

Kim, E.S., Sun, H., Park, H., Shin, S.-c., Chae, E.J., Ouderkirk, R., Bernitsas, M.M., 2021. Development of an alternating lift converter utilizing flow-induced oscillations to harness horizontal hydrokinetic energy. Renew. Sustain. Energy Rev. 145, 111094.

Larsen, C.M., Vikestad, K., Yttervik, R., Passano, E., Baarholm, G.S., 2001. VIVANA Theory Manual. Marintek, Trondheim, Norway.

Li, A., Mentzelopoulos, A., Triantafyllou, M.S., Fan, D., 2022. Dual-frequency vortex-induced vibrations of long flexible stepped cylinders. Phys. Fluids.

Lv, Y., Sun, L., Bernitsas, M.M., Sun, H., 2021. A comprehensive review of nonlinear oscillators in hydrokinetic energy harnessing using flow-induced vibrations. Renew. Sustain. Energy Rev. 150, 111388.

Morse, T., Williamson, C., 2009. The effect of Reynolds number on the critical mass phenomenon in vortex-induced vibration. Phys. Fluids 21 (4), 045105.

Park, H., Kumar, R.A., Bernitsas, M.M., 2016. Suppression of vortex-induced vibrations of rigid circular cylinder on springs by localized surface roughness at 3× 104 Re 1.2× 105. Ocean Eng. 111, 218–233.

Raghavan, K., Bernitsas, M., 2011. Experimental investigation of Reynolds number effect on vortex induced vibration of rigid circular cylinder on elastic supports. Ocean Eng. 38 (5–6), 719–731.

Raissi, M., Wang, Z., Triantafyllou, M.S., Karniadakis, G.E., 2019. Deep learning of vortex-induced vibrations. J. Fluid Mech. 861, 119–137.

Roveri, F.E., Vandiver, J.K., 2001. Using Shear7 for assessment of fatigue damage caused by current induced vibrations. In: Proc. 20^{th} OMAE Conf.. pp. 3–8.

Rudy, S., Fan, D., del Aguila Ferrandis, J., Sapsis, T.P., Triantafyllou, M.S., 2022. Optimized parametric hydrodynamic databases provide accurate response predictions and describe the physics of vortex-induced vibrations. J. Fluids Struct. 112, 103607.

Rudy, S., Fan, D., Ferrandis, J.d.A., Sapsis, T., Triantafyllou, M.S., 2021a. Learning optimal parametric hydrodynamic database for vortex-induced crossflow vibration prediction. arXiv preprint arXiv:2104.05887.

Rudy, S., Fan, D., Ferrandis, J.d.A., Sapsis, T., Triantafyllou, M.S., 2021b. Learning optimal parametric hydrodynamic database for vortex-induced crossflow vibration prediction of both freely-mounted rigid and flexible cylinders. In: The 31st International Ocean and Polar Engineering Conference. OnePetro.

Sarpkaya, T., 1978. Fluid Forces on Oscillating Cylinders. NASA STI/Recon Technical Report A, 78, pp. 275–290.

Sarpkaya, T., 1979. Vortex-induced oscillations: A selective review.

Sarpkaya, T., 1995. Hydrodynamic damping, flow-induced oscillations, and biharmonic response. J. Offshore Mech. Arct. Eng. 117 (4), 232–238.

Triantafyllou, M.S., Bourguet, R., Dahl, J., Modarres-Sadeghi, Y., 2016. Vortex-induced vibrations. In: Springer Handbook of Ocean Engineering. Springer, pp. 819–850.

Triantafyllou, M.S., Triantafyllou, G.S., Tein, Y.S., Ambrose, B.D., 1999. Pragmatic riser VIV analysis. In: Offshore Tech. Conf. Offshore Technology Conference.

Vandiver, J., 1999. SHEAR7 Program User Manual. Massachusetts Institute of Technology, Cambridge, MA.

Wang, J.-s., Fan, D., Lin, K., 2020. A review on flow-induced vibration of offshore circular cylinders. J. Hydrodyn. 32 (3), 415–440.

Wang, Z., Fan, D., Triantafyllou, M.S., 2021a. Illuminating the complex role of the added mass during vortex induced vibration. Phys. Fluids 33 (8), 085120.

Wang, Z., Fan, D., Triantafyllou, M.S., Karniadakis, G.E., 2021b. A large-eddy simulation study on the similarity between free vibrations of a flexible cylinder and forced vibrations of a rigid cylinder. J. Fluids Struct. 101, 103223.

Wang, Z., Triantafyllou, M.S., Constantinides, Y., Karniadakis, G.E., 2018. A spectral-element/Fourier smoothed profile method for large-eddy simulations of complex VIV problems. Comput. & Fluids 172, 84–96.

Willden, R.H., Graham, J.M.R., 2005. CFD simulations of the vortex-induced vibrations of model riser pipes. In: International Conference on Offshore Mechanics and Arctic Engineering, Vol. 41979. pp. 837–846.

Williamson, C.H., 1989. Oblique and parallel modes of vortex shedding in the wake of a circular cylinder at low Reynolds numbers. J. Fluid Mech. 206, 579–627.

Williamson, C.H.K., 1996. Vortex dynamics in the cylinder wake. Annu. Rev. Fluid Mech. 28 (1), 477–539.

Williamson, C.H., Govardhan, R., 2004. Vortex-induced vibrations. Annu. Rev. Fluid Mech. 36, 413–455.

Wu, W., Bernitsas, M.M., Maki, K., 2014. RANS simulation versus experiments of flow induced motion of circular cylinder with passive turbulence control at 35,000 $< ReRe <$ 130,000. J. Offshore Mech. Arct. Eng. 136 (4).

Wu, J., Yin, D., Lie, H., Riemer-Sørensen, S., Sævik, S., Triantafyllou, M., 2020. Improved VIV response prediction using adaptive parameters and data clustering. J. Mar. Sci. Eng. 8 (2), 127.

Xu, Y., Fu, S., Chen, Y., Zhong, Q., Fan, D., 2013. Experimental investigation on vortex induced forces of oscillating cylinder at high Reynolds number. Ocean Syst. Eng. 3 (3), 167–180.

Zdravkovich, M., 1996. Different modes of vortex shedding: An overview. J. Fluids Struct. 10 (5), 427–437.

Zheng, H., Price, R., Modarres-Sadeghi, Y., Triantafyllou, G.S., Triantafyllou, M.S., 2011. Vortex-induced vibration analysis (VIVA) based on hydrodynamic databases. In: International Conference on Offshore Mechanics and Arctic Engineering, Vol. 44397. pp. 657–663.